Journal Pre-proof

Non–noble Single–atom Alloy for Electrocatalytic Nitrate Reduction Using Hierarchical High–throughput Screening

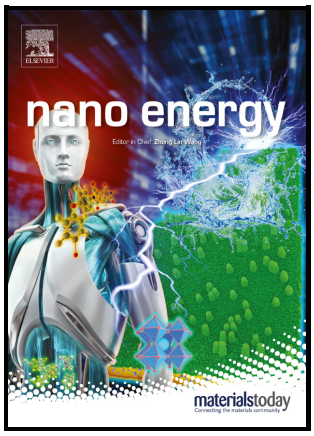

Shuo Wang, Lei Li, Kwan San Hui, Duc Anh Dinh, Zhiyi Lu, Qiuju Zhang, Kwun Nam Hui

PII: S2211-2855(23)00380-4

DOI: https://doi.org/10.1016/j.nanoen.2023.108543

Reference: NANOEN108543

To appear in: *Nano Energy*

Received date: 19 April 2023
Revised date: 7 May 2023
Accepted date: 18 May 2023

Please cite this article as: Shuo Wang, Lei Li, Kwan San Hui, Duc Anh Dinh, Zhiyi Lu, Qiuju Zhang and Kwun Nam Hui, Non–noble Single–atom Alloy for Electrocatalytic Nitrate Reduction Using Hierarchical High–throughput Screening, *Nano Energy,* (2023) doi:https://doi.org/10.1016/j.nanoen.2023.108543

Non–noble single–atom alloy for electrocatalytic nitrate reduction using hierarchical high–throughput screening

Shuo Wang[a,#], Lei Li[b,#], Kwan San Hui[c,*], Duc Anh Dinh[d], Zhiyi Lu[e,f], Qiuju Zhang[e,f*], Kwun Nam Hui[a,*]

[a] Joint Key Laboratory of the Ministry of Education, Institute of Applied Physics and Materials Engineering, University of Macau, Avenida da Universidade, Taipa, Macau SAR, P.R. China. Email: bizhui@um.edu.mo

[b] Hefei National Laboratory for Physical Sciences at the Microscale, Collaborative Innovation Center of Chemistry for Energy Materials, University of Science and Technology of China, Hefei 230026, P.R. China. Email: uestclilei@163.com

[c] School of Engineering, Faculty of Science, University of East Anglia, Norwich, NR4 7TJ, United Kingdom. Email: k.hui@uea.ac.uk

[d] NTT Hi−Tech Institute, Nguyen Tat Thanh university, Ho Chi Minh city 700000, Vietnam Email: ddanh@ntt.edu.vn

[e] Key Laboratory of Advanced Fuel Cells and Electrolyzers Technology of Zhejiang Province, Ningbo Institute of Materials Technology and Engineering, Chinese Academy of Sciences, Ningbo, Zhejiang 315201, China. E−mail: zhangqj@nimte.ac.cn

[f] University of Chinese Academy of Sciences, Beijing, 100049, China

[#] These authors contribute equally.

Abstract

Electrochemical nitrate reduction reaction (NO_3RR) holds promise for the management of wastewater contamination and synthesis of carbon−neutral ammonia (NH_3). However, high−quality catalysts with controllable reaction pathways and high activity and selectivity are still lacking. The emerging single atom alloys (SAAs) offer attractive possibilities in nitrate reduction due to their unique atomic and electronic structures. By high−throughput first−principles calculations, we explore the possible incorporation of a series of transition−metal alloyed Cu−based SAAs, referred to as TM/Cu(111), for NO_3RR toward NH_3. A hierarchical four−step screening strategy have been employed to evaluate twenty−seven SAA catalysts yielding three alloying elements (Ti, Ni and Nb) with high catalytic activity and NO_3RR selectivity. Finally, only Ni/Cu(111) possess the best activity among these three candidates because of its lowest limiting potential of −0.29 V. After

further analysis, we found that the adsorption free energy of $^{*}NO_3$ can be recognized as efficient descriptor to design and predict the NO_3RR performance of SAA. Furthermore, the Cu−based SAAs were revealed to exhibit pH dependent properties, which influence the competition between the hydrogen evolution reaction (HER) and NO_3RR. This work not only indicates the significant potential of SAA in electrocatalysis for NO_3RR to NH_3, but also highlights the important influence of pH on the activity and selectivity of catalysts under reaction conditions.

Key words: Nitrate reduction reaction; ammonia synthesis; single−atom alloy; pH influence; high−throughput calculations

1. Introduction

Ammonia (NH_3) , being an irreplaceable chemical ingredient in agriculture and industry, is essential for human life and development.[1−3] Nonetheless, the worldwide production of ammonia still relies on the traditional Haber−Bosch (HB) process, which consumes intensive energy and is accompanied by substantial emissions of carbon dioxide.[4, 5] Thus developing alternative sustainable strategies is imperative to replace the HB process. Electrochemical nitrate reduction reaction (NO_3RR), as a promising and simple route for green NH_3 synthesis, has been widely considered because of its unique advantages.[6] First, NO_3RR can effectively solve the problem of nitrate pollution in surface and groundwater. Generally, anthropogenic activities, such as the burning of fossil fuels, the overuse of nitrogen−rich fertilizers, and the discharge of wastewater, lead to the accumulation of nitrates in water. Hence, the recycling of excessive nitrate and its conversion to NH_3 via the electrochemical NO_3RR method can bring immediate economic benefits to the remediation process.[7] Second, nitrate (NO_3^-) is regarded as a more reactive nitrogen source because of the weaker N=O bond and higher solubility in electrolytes, which also lead to a simple,

efficient and controllable method for NH_3 synthesis. Finally, the NO_3RR strategy can be easily integrated into existing processes, and the production scale can be further scaled up.[8] Thus, NO_3RR can provide a sustainable alternative to the HB process while providing a solution to restore imbalances in the global nitrogen cycle.[9]

Despite this, developing highly efficient electrode materials with high selectivity and low energy consumption is still challenging because the reduction of nitrate to NH_3 is a complicated route ($NO_3^- + 9H^+ + 8e^- \rightarrow NH_3 + 3H_2O$) accompanied with several by−products (e.g., NO_2, NO, N_2, and N_2O).[10, 11] To date, significant efforts have been exerted to investigate active, selective, and stable NO_3RR electrodes.[6, 12−17] Former studies have demonstrated that Copper (Cu) shows promising performance for catalyzing NO_3RR to NH_3 in alkaline media.[8, 18, 19] Wang et. al. showed that $Cu_{50}Ni_{50}$ alloy catalysts exhibit enhanced performance for NO_3RR due to the ability of Ni to tune the Cu *d*−band center and modulate the adsorption energies of intermediates.[18] Another study reported the electroreduction of nitrate to NH_3 catalyzed by using a copper−molecular solid catalyst, achieving a maximum Faradaic efficiency of 85.9% at −0.4 V versus a reversible hydrogen electrode, which can be attributed to regulating the transfer of protons and/or electrons to the copper centres.[19] However, only when high overpotentials are supplied (around −0.4 ~ −0.7 V vs. RHE), can sufficient H coverage be ensured to improve the catalytic efficiency.[20] Then, a series of random alloys electrocatalysts (e.g., CuNi[18] and CuRh[21]) have been synthesized and applied to NO_3RR. However, maintaining the balance between high current density and Faradaic efficiency remains a challenge because of the ubiquitous adsorption–energy ratio relationship.[22] In recent years, ordered intermetallic alloys have received extensive attention to circumvent the energy−scaling limitation due to their atomically ordered structures and specified compositions.[23−25] Nevertheless, the precise synthesis of ordered intermetallic nanocrystals still faces many technical difficulties, and the

structure−activity relationship remains unexplored. Subsequently, many strategies, such as employing metal salts of various ligands,[26] or minimize the concentration of active metals,[22] have been developed to improve catalytic activity.

Single−atom alloys (SAAs) are an emerging kind of single atom catalysts (SACs) that combine the advantages of alloys and SACs and plays an increasingly important role in the field of SACs. As the name suggests, single−atom alloys (SAAs) are a class of materials where transition metals (TMs) that are active in specific reactions are dispersed on the surface of inert metal hosts (e.g. Cu, Ag, and Au).[27−29] TMs are often characterized by their excellent electronic properties due to their unique d−orbital electron arrangement, which is of great research significance in the synthesis of SAAs and in characterizing their catalytic activity. Up to now, SAAs have been widely used to promote electrocatalytic activity, which can effectively catalyze selective hydrogenations,[30, 31] C−C coupling reactions,[32] oxygen reduction,[33, 34] NO reduction,[35] CO_2 reduction,[36] nitrogen reduction[37] and CO oxidation[38], among many other reactions. Recent study has shown that dispersed gold atoms on copper Au/Cu(111) exhibit high Faradaic efficiency because of the electron migration from Cu to Au atoms creates electron−deficient Cu active sites, which promote the generation of active hydrogen species (*H) that can readily hydrogenate NO_3^-.[39] However, precious metal−based SAAs are costly and not viable for long−term sustainable solutions. Therefore, building theory−guided principles in material design is crucial to develop advanced catalytic systems for the discovery of high−performance NO_3RR electrocatalysts toward NH_3.

Inspired by these, based on first−principles calculation, we proposed a step−by−step high−throughput screening strategy that is both highly effective and inexpensive to design Cu−based SAAs with high NO_3RR performance. Here, a series of single transition metal (TM) atoms alloyed on Cu(111) are investigated, denoted as TM/Cu(111) (TM = 3d, 4d, and 5d

transition metals, as shown in Fig. 1a). In such strategy, four screening steps, including formation energies, NO_3^- adsorption energies, selectivity and activity are examined sequentially. After that, three candidates including Ti/Cu(111), Ni/Cu(111) and Nb/Cu(111), were screened out among twenty−seven SAAs, which all satisfy the given criteria. Finally, Ni/Cu(111) stands out because of the highest activity and selectivity for NO_3RR to NH_3 with the limiting potential is only −0.29 V, which is comparable or even greater than former studies of Fe SAC (−0.30 V)[13], Ru/g−C_3N_4 (−0.34 V)[40] and Os SAC (−0.42 V)[41]. We found that the adsorption of $^*NO_3$ and pH influence the activity and selectivity of NO_3RR, respectively. This work provides theoretical guidance for the rational design of SAA catalysts for NO_3RR to NH_3 and provide a stimulating impetus for further experimental exploration.

2. Results and discussion

2.1. Structure of SAAs and the Screening Strategy

In this work, single TM atoms alloyed on Cu(111)−based catalysts (denoted as TM/Cu(111)) are selected for NO_3RR to NH_3. A total of 27 SAA systems are considered here, and the structural information and computational details are shown in Fig. 1a and supporting information, respectively. Four primary target properties must be considered to determine whether a candidate can be an effective catalyst for nitrate reduction (Fig. 1b): (1) The formation energy of a single atom, E_f, which is the force that binds the core metal atom to the copper substrate, evaluates the structural stability of catalyst; (2) Gibbs absorption energy of $^*NO_3$, ΔG_{*NO3}, which is typically regarded as a prerequisite for NO_3RR, determines whether $^*NO_3$ can be adsorbed by the catalyst; (3) selectivity with suitable reaction free energy of $\Delta G_{NO3-NO3H}$ for $^*NO_3 + H^+ + e^- = {}^*NO_3H$, and ΔG_{NO-NHO} for $^*NO + H^+ + e^- = {}^*NHO$, as compared with other elementary reactions, these two elementary reactions often demand higher energy injection. In addition, good catalysts also need to resist the competitive effect

of HER. (4) Activity with low limiting potential. First, by calculating E_f, we found that the values of all systems are negative (Fig. 1c and Table S1), ranging from −0.79 to −9.82 eV, indicating that all systems are proved to be thermodynamically stable and hold great potential for experimental synthesis. According to the Bader charge analysis (Fig. S1), an electron can be easily transported between the TM and adjacent copper atoms. Moreover, the number of charge transfers in each period fluctuates from left to right, that is, from losing to gaining electrons, which may influence the adsorption and activation of $^{*}NO_3$.

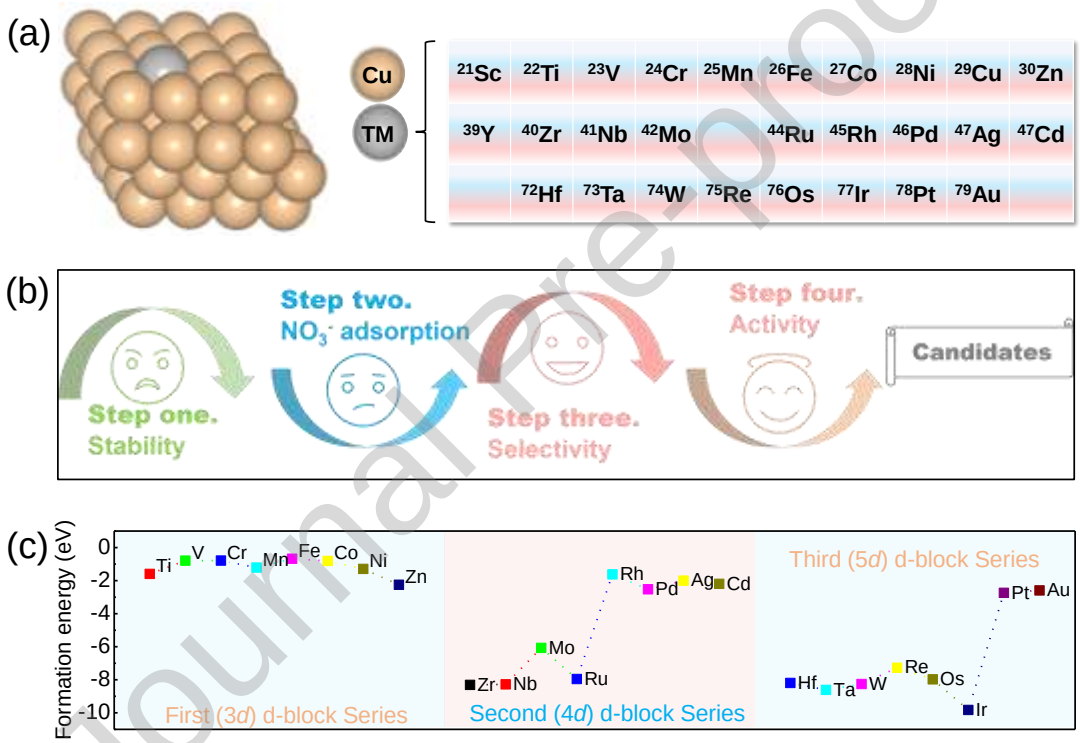

Fig. 1. (a) side view of the structural prototype of TM/Cu(111) catalysts is shown ong the left. All TM atoms considered for doping are shown on the right. (b) Four−step screening method for selecting promising TM/Cu(111) catalysts for NO_3RR to NH_3. (c) Formation energies between the TMs and the Cu substrates.

2.2. NO_3^- Adsorption and Activation on SAAs

The chemisorption and activation of NO_3^- on the electrocatalyst surfaces are critical in the NO_3RR, which play a decisive role to begin the following hydrogenation process. To

study the adsorption and activation capacity of NO_3^-, the bonding mechanism of NO_3^- must be understood first. Fig. 2a qualitatively illustrates the bonding scheme of NO_3^-. N atoms bond with O in sp^2 hybrid orbitals, and the main interaction between them involves three σ−type electron−shared bonding. Thus, a planar triangular ion is formed. At the same time, a delocalized large π bond with four centers and six electrons is formed between the three O atoms and the central N atom. The strong binding strength of transition metal active sites with NO_3^- can be attributed to their favorable combination of unoccupied and occupied d orbitals (Fig. 2b), in which the empty d−orbital can accepted the electrons from the NO_3^- wheraes the electrons from d−orbital will also back donate to the delocalized π bond and then weakened the N−O σ−bond. The nature of the interaction between TM and NO_3^- is characterized by the "acceptance−donation" of electrons, where the combination of empty and occupied d orbitals plays a critical role.

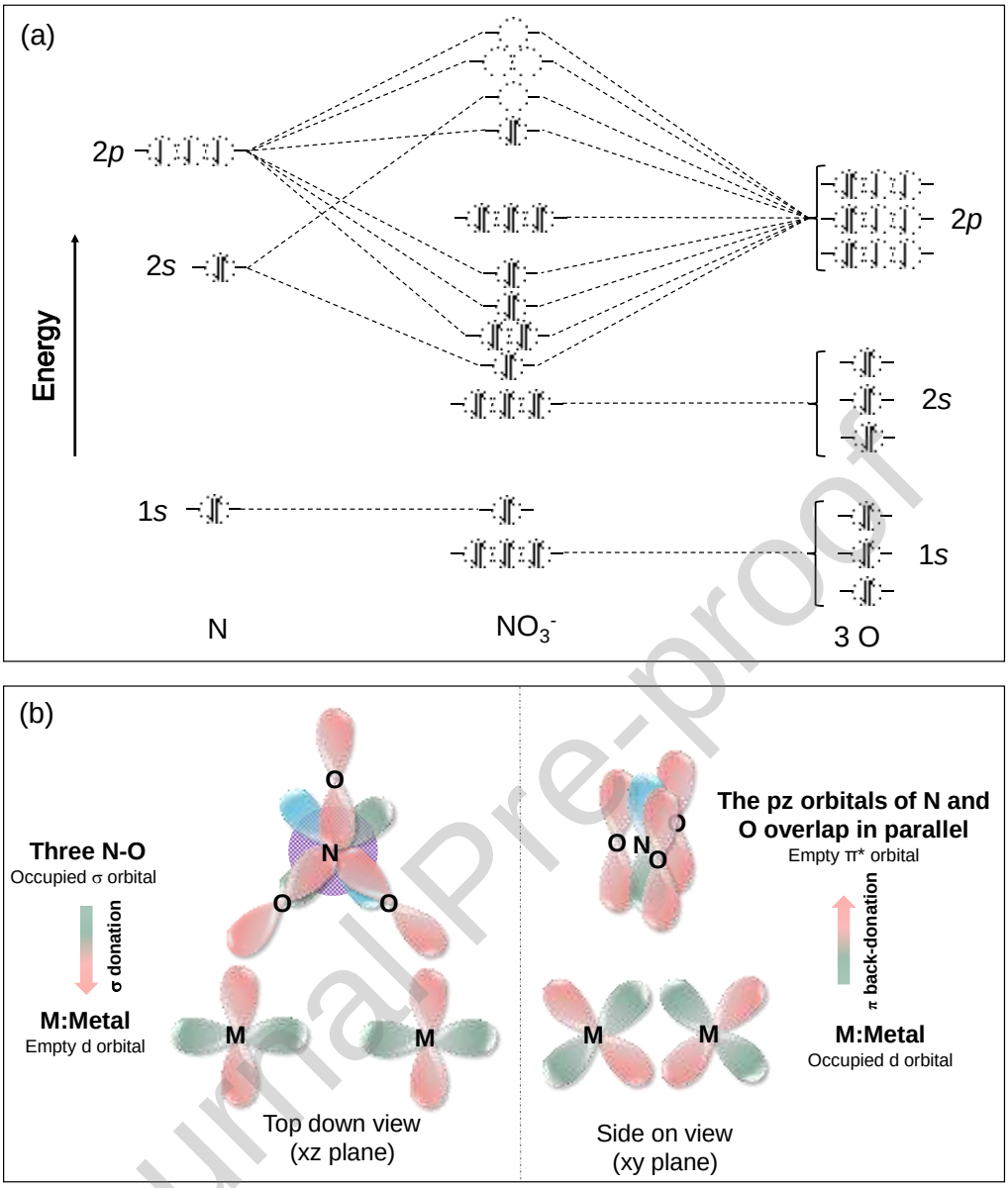

Fig. 2. (a) Bonding scheme of NO_3^-. The scheme qualitatively illustrates the bonding interactions between nitrogen 1s−2s−2p orbitals and oxygen 1s−2s−2p orbitals in the NO_3^- fragment. (b) Simplified schematic of NO_3^- bonding to TMs.

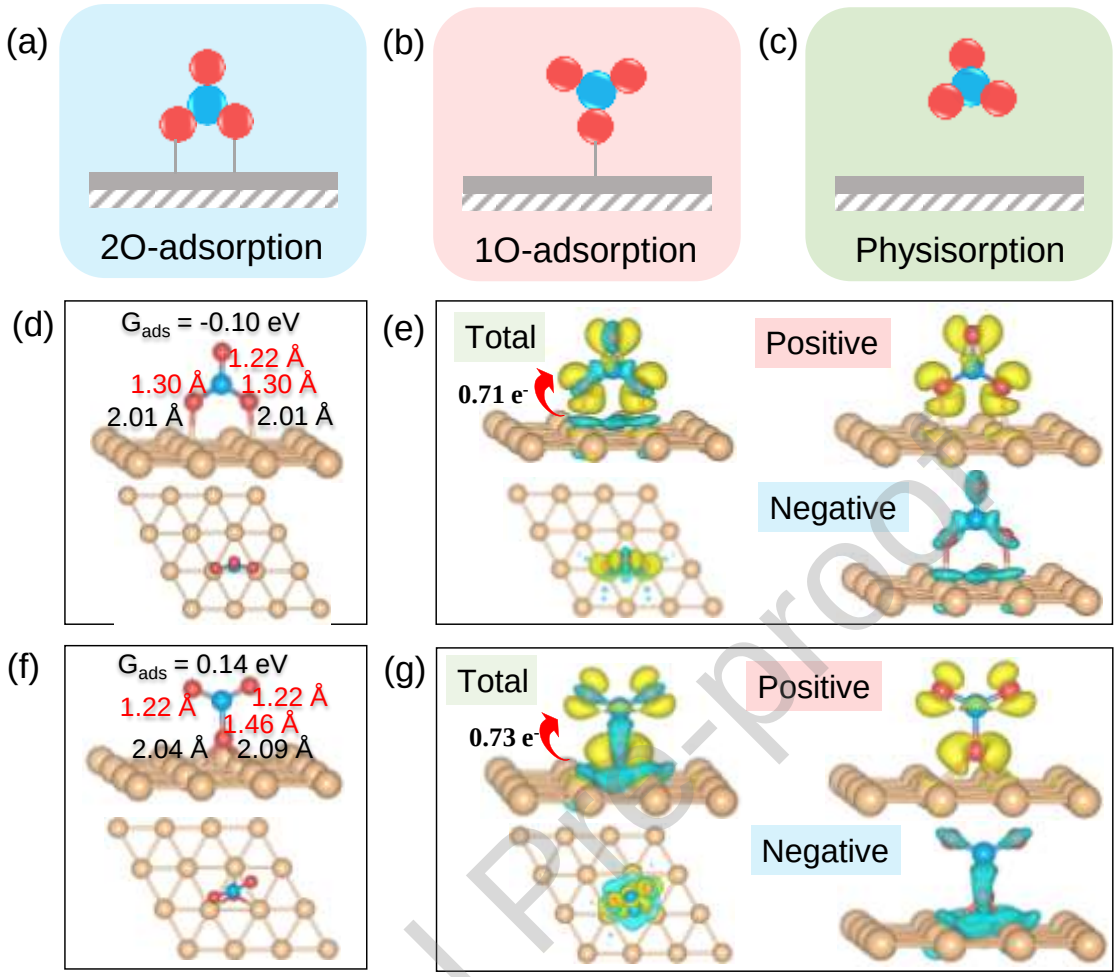

Fig. 3. (a–c) Three possible configurations of the adsorption of NO_3^- on the Cu(111) surfaces. Structural diagrams of NO_3^- adsorbed on Cu(111) through (d) 2–O and (f) 1–O adsorbed patterns. The yellow, red, and blue balls represent Cu, O, and N atoms, respectively. Charge density difference for NO_3^- adsorbed on Cu(111) through (e) 2–O and (g) 1–O patterns; the accumulation and loss of charge at an isosurface value of 0.0025 e/Å^3 are shown in yellow and blue, respectively.

Subsequently, three adsorption modes are considered. As illustrated in Fig. 3a–c, NO_3^- can be adsorbed on the active site via chemisorption (2O and 1O patterns) or physisorption. Taking Cu(111) as an example, our calculations suggest that the NO_3^- chemisorption occurs on the Cu(111) surface via 2O/1O configurations with a O–Cu bond length no more than 3Å (Figures 3d and f, respectively). For the 2O adsorption mode, two O atoms bonded to two Cu simultaneously via bridge site adsorption and the N–O bond increased to 1.30 Å (the N–O bond length in NO_3^- was 1.21 Å). Through the 1O adsorption

mode, one O atom bonds with three Cu atoms via the hollow site and the resulting N−O bond measures 1.46 Å. However, the two upper N−O bonds did not increase significantly. In addition, the Cu−O bond length of 1O adsorption mode is a little bit longer than that of 2O. Combining the results of charge density difference (CDD) in Fig. 3e and g, an obvious charge transfer between NO_3^- and the substrate is observed. Moreover, the 1O mode transfers more electrons than the 2O mode, thereby leading to a longer N−O bond length. The changes in Gibbs free energy are −0.10 (2O) and 0.14 eV (1O), which indicate that NO_3^- prefers to chemisorb on Cu(111) via 2O mode in a spontaneous process. Thus, the following analysis is mainly carried out through the 2O mode.

2.3. Screening of Efficient NO_3RR Catalysts from SAAs

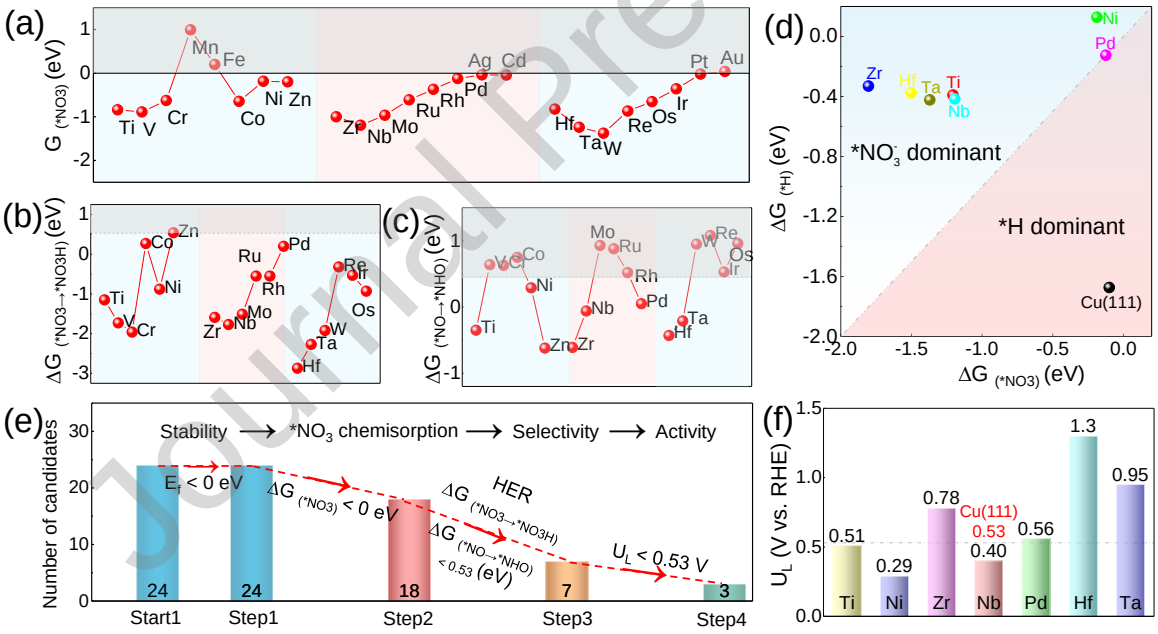

Fig. 4. Gibbs free energy changes for (a) $^*NO_3$ adsorption, (b) $^*NO_3 + H^+ + e^- \rightarrow {}^*NO_3H$, and (c) $^*NO + H^+ + e^- \rightarrow {}^*NHO$ on TM/Cu(111) surfaces. (d) Calculated $\Delta G_{(*NO3)}$ and $\Delta G_{(*H)}$. The upper left corner is the $^*NO_3$ dominant region where $\Delta G_{(*H)} > \Delta G_{(*NO3)}$. (e) Schematic of the four steps to identify promising catalysts. (f) Theoretical U_L for the surviving TM/Cu(111) catalysts.

A hierarchical method was adopted to screen out potential high−performance NO_3RR catalysts from the TM/Cu(111) systems, as shown in Fig. 4. As aforementioned, the structural stability of TM/SAA and $^*NO_3$ chemisorption are critical criteria for NO_3RR and thus are included in the screening procedure. As shown in Section 2.1, all TMs can form strong bonds with Cu(111) ($E_f < 0$), indicating that all candidates are stable through a spontaneous exothermic process. Furthermore, the Gibbs free energy changes for $^*NO_3$ adsorption on the TM/Cu(111) surfaces in Fig. 4a show that 18 candidates (Ti−, V−, Cr−, Co−, Ni−, Zn−, Zr−, Nb−, Mo−, Ru−, Rh−, Pd−, Hf−, Ta−, W−, Re−, Os−, and Ir/Cu(111)) satisfy the condition of $G_{*NO3} < 0$, which can absorb $^*NO_3$ spontaneously. Figs. 4b and 4c further depict the changes in the Gibbs free energy of the two hydrogenation processes ($^*NO_3 + H^+ + e^- \rightarrow {}^*NO_3H$, and $^*NO + H^+ + e^- \rightarrow {}^*NHO$), which are often regarded as the potential−determining steps (PDS) in NO_3RR.[40, 41] Meanwhile, the energy barrier (0.53 eV) of the PDS for the original Cu(111) is selected as a screening criteria, which will be discussed in detail in later section. This step screens 7 out of 18 TM/Cu(111) systems, namely, Ti, Ni, Zr, Nb, Pd, Hf, and Ta, to fulfill the criterion. we compared $\Delta G_{(*H)}$ and $\Delta G_{(*NO3)}$ to evaluate the selectivity of these seven TM/Cu(111),. As shown in Fig. 4d, these seven SAAs possess the negative values of $\Delta G_{(*NO3)}$, indicating that these surfaces prefer to capture nitrate rather than hydrogen and then lead to the desired NO_3RR selectivity. So far, our strategy has gradually screened seven NO_3RR candidate catalysts (Fig. 4e). Then, by calculating the hydrogenation reaction of the whole path, we finally screened three catalysts, including Ti−, Ni− and Nb/Cu(111), with lower theoretical limiting potential (U_Ls) provided in Fig. 4f, indicating that they possess good catalytic activity and selectivity. The following part will discuss more details about distinct reaction pathways.

2.4. Detailed Pathway of NO_3RR

The electrochemical reduction reaction of NO_3^- to NH_3 is a complex process with multiple reaction steps and by−products (for example, NO_2, NO, N_2O, and N_2).[17] The entire pathway from NO_3^- to NH_3, with nine protons and eight electrons transferred ($NO_3^- + 9H^+ + 8e^- \rightarrow NH_3 + 3H_2O$), is then investigated to better comprehend the NO_3RR process (Fig. 5a). The pathway includes the adsorption of NO_3^- group to form $^*NO_3$, deoxygenation of the N species, hydrogenation of the N species, and desorption of the reduced species. In addition, $^*NO$ intermediates can easily generate $^*N_2O_2$ via N–N coupling, so we also consider the main side reaction—nitrogen generation, as shown in the pink shaded part below. Then, the Gibbs free energy changes are calculated for NO_3RR of the three screened candidates (Fig. 5c−e), namely, Ti/Cu(111), Ni/Cu(111) and Nb/Cu(111), and compared with pristine Cu(111) (Fig. 5b). The structural diagrams of the corresponding NO_3RR intermediates are shown in Figs. S2−5.

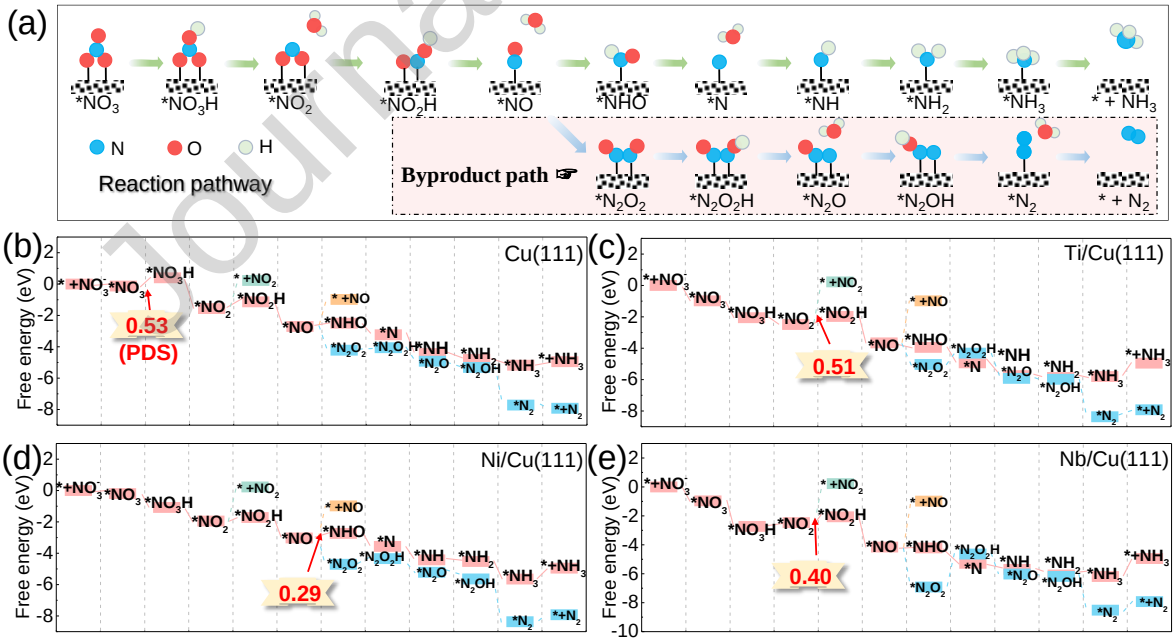

Fig. 5. (a) Reaction pathway of NO_3RR to different products. Gibbs free energy changes for NO_3RR of (b) Cu(111), (c) Cr/Cu(111), (d) Ni/Cu(111) and (e) Nb/Cu(111).

For pristine Cu(111), $^{*}NO_3$ is first adsorbed on the surface with the free energy slightly decreased by 0.12 eV. Subsequently, $^{*}NO_3$ is hydrogenated by ($H^+ + e^-$) pair to form $^{*}NO_3H$ intermediate, which is an uphill step with the free energy increasing by 0.53 eV. Then, the free energy change suddenly dropped by −1.96 eV to release first H_2O and form $^{*}NO_2$. The hydrogenation process generates $^{*}NO_2H$ through an endothermic process. Subsequently, a ($H^+ + e^-$) pair attacks $^{*}NO_2H$ accompanied with the release of second H_2O, while $^{*}NO$ remains adsorbed with the Cu–N bond. The change in the free energy profile is −1.57 eV. Next, the free energy of the endothermic process from $^{*}NO$ to $^{*}NHO$ increases by 0.21 eV. In the following steps ($^{*}NHO \rightarrow {}^{*}N$), H proton consecutively attacks $^{*}NHO$, and the corresponding energy decreases by −0.74 eV. In the subsequent steps ($^{*}N-{}^{*}NH-{}^{*}NH_2-{}^{*}NH_3$), H proton consecutively attacks intermediates, and the corresponding energies drop by −1.20, −0.37, and −0.37 eV. The energy of 0.22 eV is eventually required during the desorption of NH_3. While only 0.16 eV is demanded during the reaction steps from $^{*}NO$ to $^{*}N_2$, indicating it is prefer to produce N_2 gas on pristine Cu(111). Thus, the PDS on pristine Cu(111) is occurred on the first hydrogenation step ($^{*}NO_3 + H^+ + e^- \rightarrow {}^{*}NO_3H$) with the 0.53 eV demanded energy.

When TMs are introduced to form SAA, $^{*}NO_3$ is spontaneously adsorbed on the active site with a more negative ΔG_{*NO3} of −0.83, −0.20 and −0.96 eV for Ti−, Ni− and Nb/Cu(111), respectively, than that on pristine Cu(111) (−0.12 eV). For Ti/Cu(111), it goes through the exothermal process until $^{*}NO_2$ is formed with energy changes of −0.98 eV and −1.08 eV in each step. The following hydrogenation step ($^{*}NO_2 + H^+ + e^- \rightarrow {}^{*}NO_2H$) is upward, and the Gibbs free energy change is 0.51 eV. The next two processes are also exothermal. In the following three steps ($^{*}NHO \rightarrow {}^{*}N \rightarrow {}^{*}NH \rightarrow {}^{*}NH_2$), all are downhill, and their Gibbs free energy changes are −0.99, −0.82 and −0.11 eV, respectively. Then, the last hydrogenation step with an energy of 0.06 eV is then demanded to generate $^{*}NH_3$. The final process refers to

the release of the adsorbed NH_3 with 0.86 eV free energy changes. The PDS on Ti/Cu(111) occurrs on the formation of $^*NO_2H$ with the value of 0.51 eV. Similar reaction processes were observed on Ni− and Nb/Cu(111) catalysts, although the potential determining steps (PDSs) were found to be different. On Ni/Cu(111), the PDS occurs during *NO → *NHO conversion, with a limiting potential of 0.29 V throughout the entire reaction process for NH_3 production. However, during the hydrogenation of $^*N_2O_2$ ($^*N_2O_2 + H^+ + e^- \rightarrow {}^*N_2O_2H$), the energy input required to produce N_2 on Ni/Cu(111) must exceed 0.37 V. While the PDS of Nb/Cu(111) occurred on the formation of $^*NO_2H$ with a relatively high limiting potential of 0.40 V. Alloying the active metal on the surface of the Cu substrate can reduce the reaction energy barrier of the first hydrogenation step and also alter the PDS.

To further understand why Ni/Cu(111) exhibits higher selectivity for NH_3 synthesis than pristine Cu(111), we conducted an analysis of the bond length of the adsorbed intermediate and the CDD of $^*NH_3$ and $^*N_2$ adsorbed on Cu(111) and Ni/Cu(111). The new results are presented in Fig. S6 and Table S2. Our analysis revealed that all intermediates form shorter bonds between the N atom and the active metal site on Ni/Cu(111) than on Cu(111), suggesting that the incorporation of Ni enhances the adsorption ability of N−contained intermediates. In the case of $^*NH_3$ formation, the bond lengths (d_{N-M}) on Cu(111) and Ni/Cu(111) both increase to 2.10 Å and 2.01 Å, respectively, which is longer than the bond length (1.84 Å) between the important intermediate−$^*N$ and active sites. Furthermore, the CDD results show that there are clear charge transfers between $^*NH_3$ and the active metal on both Cu(111) and Ni/Cu(111), which facilitates the formation of NH_3 gas.

The Bader charge analysis further revealed that $^*NH_3$ gains 2.90 and 2.88 e^- when adsorbed on Cu(111) and Ni/Cu(111), respectively. When $^*N_2$ adsorbs on Ni/Cu(111), the bond length between N−Ni is 1.79 Å. According to the CDD results, $^*N_2$ remains in a strongly adsorbed state due to the significant charge transfer effect (0.27 e^-) between N and

Ni (Fig. S6b). On the other hand, when $^{*}N_2$ adsorbs on Cu(111), it spontaneously escapes from the surface as the distance between N and the surface increases to more than 3 Å, forming an isolated N_2 molecule.

In summary, while the original Cu(111) surface promotes the desorption of $^{*}N_2$, which is not conducive to NH_3 production, the incorporation of Ni strengthens adsorption of N−contained intermediates, reduces the reaction energy barrier for NH_3 formation, and makes N_2 desorption challenging. As a result, the selectivity of NO_3RR towards NH_3 is significantly improved.

Till now, only Ni/Cu(111) shows the lowest limiting potential among the two other candidates, which is also comparable or even better than previous reported DFT predicted results (Fe SAC (−0.30 V)[13], Ru/g−C_3N_4 (−0.34V)[40] and Os SAC (−0.42 V)[41], detailed data are shown in Table S3). Furthermore, the dynamic stability of Ni/Cu(111) is considered by computing the ab initio molecular dynamics (AIMD) (Fig. S7), which is a prerequisite for studying catalytic properties. After the AIMD evolved by 5,000 steps at the step length of 2 fs, the structure of Ni/Cu(111) is still stable and the value of temperature and energy oscillate around a certain value. It also possesses extraordinarily high thermal stability at 300 K. Hence, Ni/Cu(111) is finally selected as the potential NO_3RR catalyst and will be carried out for subsequent analysis.

2.5. Selectivity Evaluation and pH Influence

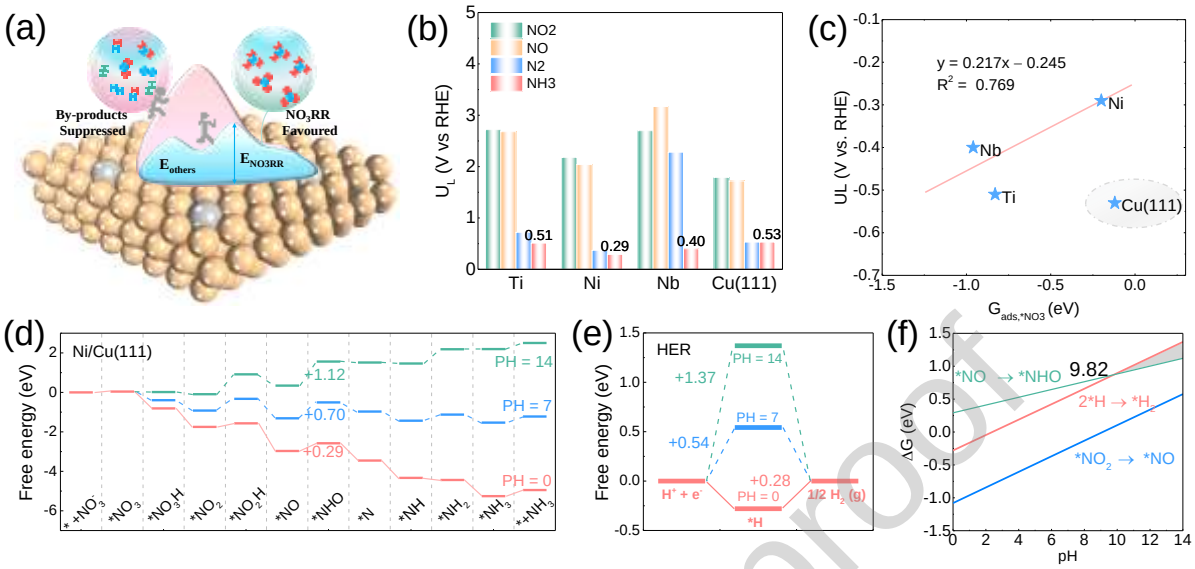

Fig. 6. (a) Schematic of the competition products between the NH_3 and by−products. (b) U_Ls for the NO_3RR of different products [$U_L(NH_3)$, $U_L(NO_2)$, $U_L(N_2)$ and $U_L(NO)$]. (c) U_Ls for the NO_3RR as a function of $^*NO_3$ adsorption energy. Detailed reaction pathways of (d) NO_3RR and (e) HER on Ni/Cu(111) at pH = 0, 7, and 14. (f) Competitive relationship of PDS between NO_3RR and HER in all pH region.

Apart from the catalytic activity discussed above, selectivity, which will affect the reaction efficiency of NO_3RR, is also an essential feature to consider when evaluating a catalyst, (Fig. 6a). Here, to compare the selectivity of the TM/Cu(111) catalysts, the limiting potentials (U_L) for the production of NH_3 and other by−products are summarized in Fig. 6b and Table S4. All three candidates show the lowest U_Ls to produce NH_3, indicating that it is relatively challenging for the formation of by−products, such as NO_2, NO, and N_2. Hence, it is reasonable to assume that the final synthesis of NH_3 is possible. Fig. 6c depicts the changes in U_Ls in relation to the $^*NO_3$ adsorption energies to help us fully comprehend the catalytic mechanism. Interestingly, apart from pristine Cu(111), the U_Ls of all TM/Cu(111) candidates are linearly related to the $^*NO_3$ adsorption energies, which is consistent with previous studies.[17, 41] In this work, weaker $^*NO_3$ adsorption will lead to lower U_L and thus higher efficiency of NO_3RR to NH_3.

Considering that NO_3RR occurs in a liquid phase, we must also additionally consider the influence of the electrolyte environment on catalytic performance. Hence, the influence of pH on the reaction pathways of the selected Ni/Cu(111) is further explored, and the free energy evolution plots of NO_3RR and HER at pH = 7 and 14 are considered, as shown in Fig. 6d and 6e, respectively. In order to compare the limiting potential of the PDS between NO_3RR (ΔG_{PDS}) and HER (ΔG_{H2}), former results determined the PDS of Ti/Cu(111) and Nb/Cu(111) to occur during $^*NO_2 + H^+ + e^- \rightarrow {}^*NO_2H$, as shown in Figs. 5c and e, while the PDS of Ni/Cu(111) occurs during $^*NO + H^+ + e^- \rightarrow {}^*NHO$ (Fig. 5d). We selected these two PDSs ($^*NO_2 + H^+ + e^- \rightarrow {}^*NO_2H$ and $^*NO + H^+ + e^- \rightarrow {}^*NHO$) as evaluation indicators to assess the influence of pH. Additionally, to align with a previous study[42], we selected the continuous two−step hydrogenation reaction of $^*NO_2$ ($^*NO_2 + 2H^+ + 2e^- \rightarrow {}^*NO$) on Ni/Cu(111) as an indicator, shown in Fig. 6f. The free energies of intermediates change to higher energies as the concentration of H^+ increases, whereas the PDS of NO_3RR is still maintain unchanged (Fig. 6d). For example, the U_L of NO_3RR increases to 0.70 V in the neutral environment (pH = 7). The formation energy of H_2 is 0.54 eV, which is larger than that of the adsorption of NO_3^- (−0.20 eV) while lower than the U_L (0.70 V) of NO_3RR, resulting in poor performance of NO_3RR. However, in an alkaline environment (pH = 14), the U_L of NO_3RR increase to 1.12 V, which is lower than that of HER, 1.37 eV, thereby improving NO_3RR due to the inhibited HER. The results of reaction pathways at different pH indicate that the NO_3RR pathway shows the best performance in alkaline electrolytes. To explore the selectivity of NO_3RR at a specific pH value, we further summarized the pH−dependent relationship between NO_3RR and HER on Ni/Cu(111) and compared it with Cu (Fig. S8). According to the analysis of aforementioned free energy pathways, the relationship between ΔG_{PDS} (related to PDS for generating NH_3) and pH can be obtained (Fig. 6f). For Ni/Cu(111), the shaded zone established by HER, $^*NO \rightarrow {}^*NHO$, and pH upper limit, pH = 14, which is favorable

to NO_3RR. In the zone with the pH value ranging from 9.82 to 14, ΔG_{H2} is larger than any ΔG_{PDS} in NO_3RR, indicative that the NO_3RR is more competitive than the HER, thereby leading to NO_3RR being superior than HER. Hence, the selectivity of the reaction changes upon the pH values: the production of H_2 is dominated at 0 to 9.82 and the NH_3 is mainly generated at 9.82 to 14 with the PDS occurred on the hydrogenation of $^*NO_2$. Besides, for Cu(111), the influence point of pH is 8.95, that is, NO_3RR can effectively inhibit HER in the pH range of 8.95 to 14, and the PDS is also controlled by $^*NO_3 \rightarrow {}^*NO_3H$. Thus, the competitive effect of HER can be effectively reduced for Cu−based catalyst materials at relatively high pH under alkaline conditions, which also explains why the majority of experimental NO_3RR tests are conducted in alkaline electrolytes.[16, 43]

3. Conclusion

In conclusion, high−throughput first−principles calculations are performed to investigate the activity and selectivity of TM/Cu(111) catalysts for the reduction of electrocatalytic nitrate to NH_3. Four−step criteria are used to determine whether TM/Cu(111) catalysts are adequate for converting nitrate to NH_3: (1) the stability of TM alloyed on Cu(111), (2) the Gibbs adsorption energy of NO_3^- must be satisfied ($\Delta G_{*NO3} < 0$), and (3) the U_L of PDSs should be met ($\Delta G < 0.53$ V). Most TM/Cu(111) catalysts are eliminated by these three screening criteria, remaining just seven TM/Cu(111) catalysts (TM = Ti, Ni, Zr, Nb, Pd, Hf, and Ta) that can also successfully inhibit the competing HER. By comparing the U_Ls of the seven candidates, Ti−, Ni− and Nb/Cu(111) stand out, and only Ni/Cu(111) shows the lowest limiting potential of −0.29 V and the highest selectivity compared with the production of N_2, NO and NO_2. Furthermore, we have clarified that the activity of the three candidates maintains a strong relationship with $^*NO_3$ adsorption. Ultimately, pH value has been evaluated and shows a significant impact on the catalytic activity and selectivity of NO_3RR.

We believe that this work could stimulate a different perspective towards achieving efficient nitrate−to−ammonia electrocatalysts.

Acknowledgements

This work was funded by the Science and Technology Development Fund, Macau SAR (File no. 0046/2019/AFJ and 0007/2021/AGJ), University of Macau (File no., MYRG2020−00187−IAPME and MYRG2022−00223−IAPME), the UEA funding, the Strategic Priority Research Program of the Chinese Academy of Sciences, (Grant No. XDB0450401), and Natural Science Foundation of Zhejiang Province (LY21B030006). The DFT calculations are performed at High Performance Computing Cluster (HPCC) of Information and Communication Technology Office (ICTO) at University of Macau.

References

[1] Licht, S.; Cui, B.; Wang, B.; Li, F.−F.; Lau, J.; Liu, S. Ammonia synthesis by N_2 and steam electrolysis in molten hydroxide suspensions of nanoscale Fe_2O_3, Science 345 (6197) (2014) 637−640.

[2] Guo, W.; Zhang, K.; Liang, Z.; Zou, R.; Xu, Q. Electrochemical nitrogen fixation and utilization: theories, advanced catalyst materials and system design, Chem. Soc. Rev. 48 (24) (2019) 5658−5716.

[3] Kyriakou, V.; I., G.; A., V.; E., V.; M., S. An electrochemical Haber−Bosch process, Joule 4 (2020) 1−17.

[4] Lim, J.; Fernández, C. A.; Lee, S. W.; Hatzell, M. C. Ammonia and nitric acid demands for fertilizer use in 2050, ACS Energy Lett. 6 (10) (2021) 3676−3685.

[5] Ashida, Y.; Arashiba, K.; Nakajima, K.; Nishibayashi, Y. Molybdenum−catalysed ammonia production with samarium diiodide and alcohols or water, Nature 568 (7753) (2019) 536−540.

[6] Zhang, X.; Wang, Y.; Liu, C.; Yu, Y.; Lu, S.; Zhang, B. Recent advances in non−noble metal electrocatalysts for nitrate reduction, Chem. Eng. J. 403 (2021).

[7] Su, L.; Han, D.; Zhu, G.; Xu, H.; Luo, W.; Wang, L.; Jiang, W.; Dong, A.; Yang, J. Tailoring the assembly of iron nanoparticles in carbon microspheres toward high−performance electrocatalytic denitrification, Nano Lett. 19 (8) (2019) 5423−5430.

[8] Wang, Y. T.; Zhou, W.; Jia, R. R.; Yu, Y. F.; Zhang, B. Unveiling the activity origin of a Copper−based electrocatalyst for selective nitrate reduction to ammonia, Angew. Chem. Int. Ed. 59 (13) (2020) 5350−5354.

[9] Liu, H.; Lang, X.; Zhu, C.; Timoshenko, J.; Ruscher, M.; Bai, L.; Guijarro, N.; Yin, H.; Peng, Y.; Li, J.; Liu, Z.; Wang, W.; Cuenya, B. R.; Luo, J. Efficient electrochemical nitrate reduction to ammonia with copper−supported Rhodium cluster and single−atom catalysts, Angew. Chem. Int. Ed. 61 (23) (2022) e202202556.

[10] Wang, Y.; Wang, C.; Li, M.; Yu, Y.; Zhang, B. Nitrate electroreduction: mechanism insight, in situ characterization, performance evaluation, and challenges, Chem. Soc. Rev. 50 (12) (2021) 6720−6733.

[11] van Langevelde, P. H.; Katsounaros, I.; Koper, M. T. M. Electrocatalytic nitrate reduction for sustainable ammonia production, Joule 5 (2) (2021) 290−294.

[12] Xu, H.; Ma, Y.; Chen, J.; Zhang, W.−x.; Yang, J. Electrocatalytic reduction of nitrate – a step towards a sustainable nitrogen cycle, Chem. Soc. Rev. 51 (7) (2022) 2710−2758.

[13] Wu, Z. Y.; Karamad, M.; Yong, X.; Huang, Q.; Cullen, D. A.; Zhu, P.; Xia, C.; Xiao, Q.; Shakouri, M.; Chen, F. Y.; Kim, J. Y. T.; Xia, Y.; Heck, K.; Hu, Y.; Wong, M. S.; Li, Q.; Gates, I.; Siahrostami, S.; Wang, H. Electrochemical ammonia synthesis via nitrate reduction on Fe single atom catalyst, Nat. Commun. 12 (1) (2021) 2870.

[14] Wu, J.; Li, J.−H.; Yu, Y.−X. Theoretical exploration of electrochemical nitrate reduction reaction activities on transition−metal−doped h−BP, J. Phys. Chem. Lett. 12 (16) (2021) 3968−3975.

[15] Lv, X.; Mou, T.; Li, J.; Kou, L.; Frauenheim, T. Tunable surface chemistry in heterogeneous bilayer single - atom catalysts for electrocatalytic NOx reduction to ammonia, Adv. Funct. Mater. 32 (28) (2022) 1−9.

[16] McEnaney, J. M.; Blair, S. J.; Nielander, A. C.; Schwalbe, J. A.; Koshy, D. M.; Cargnello, M.; Jaramillo, T. F. Electrolyte engineering for efficient electrochemical nitrate reduction to ammonia on a Titanium electrode, ACS Sustain. Chem. Eng. 8 (7) (2020) 2672−2681.

[17] Niu, H.; Zhang, Z.; Wang, X.; Wan, X.; Shao, C.; Guo, Y. Theoretical insights into the mechanism of selective nitrate - to - ammonia electroreduction on single - atom catalysts, Adv. Func. Mater. 31 (11) (2020) 1−8.

[18] Wang, Y.; Xu, A.; Wang, Z.; Huang, L.; Li, J.; Li, F.; Wicks, J.; Luo, M.; Nam, D.−H.; Tan, C.−S.; Ding, Y.; Wu, J.; Lum, Y.; Dinh, C.−T.; Sinton, D.; Zheng, G.; Sargent, E. H. Enhanced nitrate−to−ammonia activity on Copper–Nickel alloys via tuning of intermediate adsorption, J. Am. Chem. Soc. 142 (12) (2020) 5702−5708.

[19] Chen, G.; Yuan, Y.; Jiang, H.; Ren, S.; Ding, L.−X.; Ma, L.; Wu, T.; Lu, J.; Wang, H. Electrochemical reduction of nitrate to ammonia via direct eight−electron transfer using a copper–molecular solid catalyst, Nat. Energy 5 (8) (2020) 605−613.

[20] Liu, J.−X.; Richards, D.; Singh, N.; Goldsmith, B. R. Activity and selectivity trends in electrocatalytic nitrate reduction on transition metals, ACS catal. 9 (8) (2019) 7052−7064.

[21] Mirzaei, P.; Bastide, S.; Aghajani, A.; Bourgon, J.; Zlotea, C.; Laurent, M. P.; Latroche, M.; Cachet−Vivier, C. J. E. Electrocatalytic reduction of nitrate and nitrite at CuRh nanoparticles/C nomposite electrodes, Electrocatalysis 9 (2018) 343−351.

[22] Gao, Q.; Pillai, H. S.; Huang, Y.; Liu, S.; Mu, Q.; Han, X.; Yan, Z.; Zhou, H.; He, Q.; Xin, H.; Zhu, H. Breaking adsorption−energy scaling limitations of electrocatalytic nitrate reduction on intermetallic CuPd nanocubes by machine−learned insights, Nat. Commun. 13 (1) (2022) 2338.

[23] Jiang, K.; Wang, P.; Guo, S.; Zhang, X.; Shen, X.; Lu, G.; Su, D.; Huang, X. Ordered PdCu−based nanoparticles as bifunctional oxygen−reduction and ethanol−oxidation electrocatalysts, Angew. Chem. Int. Ed. 55 (31) (2016) 9030−5.

[24] Kim, D.; Xie, C.; Becknell, N.; Yu, Y.; Karamad, M.; Chan, K.; Crumlin, E. J.; Nørskov, J. K.; Yang, P. Electrochemical activation of CO(2) through atomic ordering transformations of AuCu nanoparticles, J. Am. Chem. Soc. 139 (24) (2017) 8329−8336.

[25] Wang, C.; Chen, D. P.; Sang, X.; Unocic, R. R.; Skrabalak, S. E. Size−dependent disorder−order transformation in the synthesis of monodisperse intermetallic PdCu nanocatalysts, ACS Nano 10 (6) (2016) 6345−6353.

[26] Shimbayashi, T.; Fujita, K.−i. Recent advances in homogeneous catalysis via metal–ligand cooperation involving aromatization and dearomatization, Catalysts 10 (6) (2020) 635.

[27] Darby, M. T.; Stamatakis, M.; Michaelides, A.; Sykes, E. C. H. Lonely atoms with special gifts: Breaking linear scaling relationships in heterogeneous catalysis with single−atom alloys, J. Phys. Chem. Lett. 9 (18) (2018) 5636−5646.

[28] Hannagan, R. T.; Giannakakis, G.; Flytzani−Stephanopoulos, M.; Sykes, E. C. H. Single−atom alloy catalysis, Chem. Rev. 120 (21) (2020) 12044−12088.

[29] Shen, T.; Wang, S.; Zhao, T.; Hu, Y.; Wang, D. Recent advances of single - atom - alloy for energy electrocatalysis, Adv. Energy Mater. (2022).

[30] Pei, G. X.; Liu, X. Y.; Wang, A.; Lee, A. F.; Isaacs, M. A.; Li, L.; Pan, X.; Yang, X.; Wang, X.; Tai, Z.; Wilson, K.; Zhang, T. Ag alloyed Pd single−Atom catalysts for efficient selective hydrogenation of acetylene to ethylene in excess ethylene, ACS Catal. 5 (6) (2015) 3717−3725.

[31] Liu, J.; Uhlman, M. B.; Montemore, M. M.; Trimpalis, A.; Giannakakis, G.; Shan, J.; Cao, S.; Hannagan, R. T.; Sykes, E. C. H.; Flytzani−Stephanopoulos, M. Integrated catalysis−surface science−theory approach to understand selectivity in the hydrogenation of 1−Hexyne to 1−Hexene on PdAu single−atom alloy catalysts, ACS Catal. 9 (9) (2019) 8757−8765.

[32] Réocreux, R.; Uhlman, M.; Thuening, T.; Kress, P.; Hannagan, R.; Stamatakis, M.; Sykes, E. C. H. Efficient and selective carbon–carbon coupling on coke−resistant PdAu single−atom alloys, Chem. Commun. 55 (100) (2019) 15085−15088.

[33] Zhang, L.; Liu, H.; Liu, S.; Norouzi Banis, M.; Song, Z.; Li, J.; Yang, L.; Markiewicz, M.; Zhao, Y.; Li, R.; Zheng, M.; Ye, S.; Zhao, Z.−J.; Botton, G. A.; Sun, X. Pt/Pd Single−atom alloys as highly active electrochemical catalysts and the origin of enhanced activity, ACS Catal. 9 (10) (2019) 9350−9358.

[34] Jirkovský, J. S.; Panas, I.; Ahlberg, E.; Halasa, M.; Romani, S.; Schiffrin, D. J. Single atom hot−spots at Au–Pd nanoalloys for electrocatalytic H_2O_2 production, J. Am. Chem. Soc. 133 (48) (2011) 19432−19441.

[35] Xing, F.; Jeon, J.; Toyao, T.; Shimizu, K.−i.; Furukawa, S. J. C. s. A Cu–Pd single−atom alloy catalyst for highly efficient NO reduction, Chem. Sci. 10 (36) (2019) 8292−8298.

[36] Feng, Y.; An, W.; Wang, Z.; Wang, Y.; Men, Y.; Du, Y. Electrochemical CO_2 reduction reaction on M@Cu(211) bimetallic single−atom surface alloys: mechanism, kinetics, and catalyst screening, ACS Sustainable Chem. Eng. 8 (1) (2020) 210−222.

[37] Zheng, G.; Li, Y.; Qian, X.; Yao, G.; Tian, Z.; Zhang, X.; Chen, L. High−throughput screening of a single−atom alloy for electroreduction of dinitrogen to ammonia, ACS Appl. Mater. Inter. 13 (14) (2021) 16336−16344.

[38] Gao, F.; Wang, Y.; Goodman, D. W. CO oxidation over AuPd(100) from ultrahigh vacuum to near−atmospheric pressures: The critical role of contiguous Pd atoms, J. Am. Chem.Soc. 131 (16) (2009) 5734−5735.

[39] Zhang, Y.; Chen, X.; Wang, W.; Yin, L.; Crittenden, J. C. Electrocatalytic nitrate reduction to ammonia on defective Au1Cu (111) single−atom alloys, Appl. Catal. B Environ. 310 (121346) (2022) 1−11.

[40] Lv, L.; Shen, Y.; Liu, J.; Meng, X.; Gao, X.; Zhou, M.; Zhang, Y.; Gong, D.; Zheng, Y.; Zhou, Z. Computational screening of high activity and selectivity TM/g−C_3N_4 single−atom catalysts for electrocatalytic reduction of nitrates to ammonia, J. Phys. Chem. Lett. 12 (45) (2021) 11143−11150.

[41] Wang, S.; Gao, H.; Li, L.; Hui, K. S.; Dinh, D. A.; Wu, S.; Kumar, S.; Chen, F.; Shao, Z.; Hui, K. N. High−throughput identification of highly active and selective single−atom catalysts for electrochemical ammonia synthesis through nitrate reduction, Nano Energy 100 (2022) 107517, 1−9.

[42] Hu, T.; Wang, C.; Wang, M.; Li, C. M.; Guo, C. Theoretical insights into superior nitrate reduction to ammonia performance of Copper catalysts, ACS Catal. 11 (23) (2021) 14417−14427.

[43] Fan, K.; Xie, W.; Li, J.; Sun, Y.; Xu, P.; Tang, Y.; Li, Z.; Shao, M. Active hydrogen boosts electrochemical nitrate reduction to ammonia, Nat. Commun. 13 (1) (2022) 7958,1−13.

The information of each author

Shuo Wang received her M.S. degree in 2019 from Department of Chemistry, Liaoning University and Ph.D. degree in 2022 at Institute of Applied Physics and Materials Engineering, University of Macau. She is currently a postdoctoral researcher at Dalian National Laboratory for Clean Energy, Dalian Institute of Chemical Physics, Chinese Academy of Sciences. Her research mainly focuses on the single atom catalysts for the catalytic conversion process and design of novel functional materials by first principle calculation simulation.

Lei Li received his B.S degree in 2017 from Department of Materials and Chemistry and Chemical Engineering, Chengdu University of Technology, and M.S. degree in 2020 from Department of Materials and Energy, University of Electronic Science and Technology of China. Now, he is a Ph.D. candidate at University of Science and Technology of China. His topics are the theoretical prediction and design of new energy materials and catalysts.

Kwan San Hui is a Reader in Mechanical Engineering of School of Engineering, University of East Anglia. He obtained his Ph.D. degree in mechanical engineering at the Hong Kong University of Science and Technology (2008). His research focuses on advanced materials for energy storage, conversion and electrocatalysis.

Duc Anh Dinh received his PhD degree in the field of Chemistry of Materials at Italian Institute of Technology and Genova University, Italy in 2018. Currently, he is a researcher, working at Nguyen Tat Thanh hi-Tech Institute, Nguyen Tat Thanh University Vietnam. His research interest is focusing in two fields: (1) production and processing of graphene and related two dimensional materials for energy storage, sensors and electronic devices; (2) synthesis and characterization of biodegrade polymers.

Zhiyi Lu is a Professor of Key Laboratory of Advanced Fuel Cells and Electrolyzers Technology of Zhejiang Province, Ningbo Institute of Material Technology and Engineering, Chinese Academy of Sciences. He obtained his Ph.D degree from the Beijing University of Chemical Technology, China (2015). His research interest covers multi-scale surface interface regulation of low-cost electrocatalytic electrodes.

Qiuju Zhang is a Project Professor of Key Laboratory of Advanced Fuel Cells and Electrolyzers Technology of Zhejiang Province, Ningbo Institute of Material Technology and Engineering, Chinese Academy of Sciences. She obtained her Ph.D degree from the Chinese University of Hong Kong (2008). Her research focuses on electrochemical materials design and mechanism exploration.

Kwun Nam Hui is an Associate Professor of the Institute of Applied Physics and Materials Engineering, University of Macau. He obtained his Ph.D. degree from The University of Hong Kong (2009). His research focuses on electrochemical energy storage and conversion.

Graphical abstract

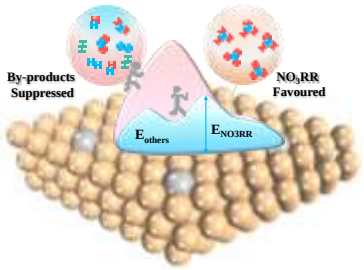

Ni/Cu(111) achieved the high performance for NH_3 production of nitrate reduction reaction after investigating a series of single atom alloys via high-throughput density functional theory calculations.

CRediT authorship contribution statement

Shuo Wang carried out the theoretical calculations and wrote the manuscript. **Shuo Wang** and **Lei Li** contribute equally. **Kwan San Hui**, **Qiuju Zhang**, **Kwun Nam Hui** conceived the idea writing-review & editing. **Duc Anh Dinh** and **Zhiyi Lu** contributed to the methodology and project design. All authors were involved in the analysis and discussion of the results.

Declaration of interests

☒ The authors declare that they have no known competing financial interests or personal relationships that could have appeared to influence the work reported in this paper.

☐The authors declare the following financial interests/personal relationships which may be considered as potential competing interests:

Highlights

- High-throughput DFT screening of single-atom alloy candidates
- Ni/Cu(111) exhibited an outstanding performance
- The adsorption of $^{*}NO_3$ and pH influence the activity and selectivity of NO_3RR